Alexandria Engineering Journal (2022) 61, 4371–4388

HOSTED BY

Alexandria University

Alexandria Engineering Journal

www.elsevier.com/locate/aej
www.sciencedirect.com

Hydraulic characterization of Diesel, B50 and B100 using momentum flux

Muhammad Numan Atique [a], S. Imran [a], Luqman Razzaq [a], M.A. Mujtaba [a,*], Saad Nawaz [a], M.A. Kalam [b,*], Manzoore Elahi M. Soudagar [b], Abrar Hussain [c], Ibham Veza [d], Attique Arshad [a]

[a] Department of Mechanical Engineering, University of Engineering and Technology (City Campus), Lahore, Pakistan
[b] Center for Energy Science, Department of Mechanical Engineering, University of Malaya, Kuala Lumpur 50603, Malaysia
[c] Department of Mechanical and Industrial Engineering, Tallinn University of Technology, Ehitajate Tee 5, 12616 Tallinn, Estonia
[d] Automotive Development Centre, School of Mechanical Engineering, Faculty of Engineering, Universiti Teknologi Malaysia, 81310 Johor Bahru, Malaysia

Received 14 July 2021; revised 12 September 2021; accepted 27 September 2021
Available online 09 October 2021

KEYWORD

Diesel;
B50;
B100;
Mass flow rate;
Momentum flux

Abstract Liquid fossil fuels are the main source of energy in transportation vehicles and aviation for many decades. This dependence on fossil fuels can be reduced by liquid biofuels blended with fossil fuels or utilized purely. The purpose of this research is to authenticate a method for different fuels for measurement of injection rate based on the spray momentum measurement and total fuel mass injected. So, in this research B50, B100 and simple diesel fuel hydraulic behavior was investigated. All the measurements have been taken in a chamber/cylinder filled with nitrogen gas at high pressure, which results in the gas density of 22.7kg/m^3 and 34.6kg/m^3, using the injection pressures 600, 800 and 1000 bar. Spray angle and spray tip penetration measurements presented that an increment in injection pressure boosted fuel spray dispersion whereas increment in ambient pressure showed a reverse effect. All fuels have almost same momentum flux for their regarding conditions. B50 and B100 have a greater momentum efficiency than simple Diesel. Momentum flux increases to a factor of almost 1.4 with every 200 bar rise in injection pressure. The fuel mass injected showed a reduction in fuel mass for B50 2–3% and for B100 5–6% as compared to diesel fuel.

1. Introduction

The global use of diesel engines have increased the pollution problems as they emit higher discharges of PM, nitrogen oxides NOx and smoke as compared with SI engine [1,2]. The internal combustion engine are leading to the motive supremacy across the world with developing states feeding increas-

* Corresponding authors.
E-mail addresses: m.mujtaba@uet.edu.pk (M.A. Mujtaba), kalam@um.edu.my (M.A. Kalam).
Peer review under responsibility of Faculty of Engineering, Alexandria University.

https://doi.org/10.1016/j.aej.2021.09.064

ing demand for automobiles, hence large number of IC engines are in working and continues to rise. China sets an admirable example to establish the worldwide progress in demand of automobiles in previous few years where marketplace of vehicles rose up to the factor of 19 between 1995 and 2012 from 0.54 to 9.50 million passenger vehicles sold in a year [3]. The overarching statistic regarding this increase in demand and dependence on the derived fossil fuels is a limited nature resource and probability of reaching topmost oil production. The peak oil production is a model that was recognized in earlier era of crude oil manipulation and is described as a spot at which production of conventional fuel will gain its peak in a specific time after that it will decrease enduringly [4]. There is plentiful guesswork as to at what time the point will take place, with hopeful rights falling in 2040 s.

Transportation and lower capacity power plants are promoting the use of biofuels and also international legislations are endorsing the use of bio fuels [5]. So it is recognized that it is necessary to use biofuels efficiently as much as we can do by introducing an optimum fuel injection strategy along with possible substitutes to swap with fossil fuels [5,6]. There are some factors on which performance of any specific fuel depends. One of the key factor is atomization of fuel in DI diesel engines to increase fuel combustion efficiency and to lessen exhaust emissions [7–9]. Selecting between the different injections strategies is an effective way to lessen exhaust emissions [10]. For example by increasing injection pressure fuel atomization can be improved and this subsequently improve combustion, which results rise in break thermal efficiency and generating less HC, CO and PM [11–13].

Biofuel is first selection of researchers between all alternate fuels because it generates less greenhouse gases, soot and smoke emissions [14]. Biodiesel contain greater oxygen content that results in the complete burning of carbon [15]. In addition biofuels are more sustainable and economical as compared with conventional fuels [16]. Biodiesel is renewable and biodegradable fuel that has a greater flashpoint than diesel whereas decreasing most of the exhaust emissions [13,14].

Research scholars perform experimentation and simulate the study for diesel engines using biodiesel produced from animal fat and different vegetable oils [12–15]. Generally biodiesel has greater viscosity and density as compared to the diesel because it is mixture of several organic molecules described by larger molecular mass, so cavitation and evaporation characteristics are different to petroleum diesel [15–17]. It was observed that the injection system was seriously affected by greater viscosity and biofuel density [18,22,23]. Different fuels show different spray characteristics, atomization process and evaporation which in advance leads to difference in combustion performance and exhaust emissions. All kinds of fuel tested on diesel engine shows that combustion characteristics are influenced by injection factors like the injection pressure, injection timing and nozzle cone angle [28]. In general hydraulic characterization is mandatory to find optimum injection technique for any engine and for every type of fuel [29].

The work shown in this current paper applies the momentum flux measurement techniques to by varying different injection parameters. As biodiesel and its blends have been recognized as a best substitute of diesel fuel. In current paper three fuels B50, B100 and pure diesel are selected for hydraulic characterization. The reason behind the selection of B50 and B100 is to get a trending behavior as biodiesel content increases in blends. The strategy has been implemented for hydraulic characterization of injection systems using momentum-flux($\dot{M}$), mass flow rate, instantaneous mass flow rate ($\dot{m}$), injection velocity and discharge coefficient. Two dimensionless factors the momentum efficiency and the momentum coefficient are announced to characterize an injection system as an alternative way. This paper also includes investigation of injection pressure, nozzle cone angle and number of holes effect on atomization of diesel and biodiesel.

2. Materials and methods

2.1. Biodiesel

The work described here is initiated from waste cooking oil collected from five different cafeterias. All suspended particles from waste cooking oil were eliminated using the filter paper of 10.5*mm* diameter. Filtered cooking oil was heated to temperature of 100 °C for 1 h to eliminate the humidity followed by the cooling process. The high speed diesel fuel for preparing the diesel–biodiesel combinations was purchased from PSO. Ethanol, methanol, potassium hydroxide, phenolphthalein and sulphuric acid were bought from Sigma Aldrich.

The free fatty-acid (FFA) level for raw WCO was found to be 3.9 mg KOH/g, such high values for FFA is usually associated with long chain molecules and is reported not suitable for transesterification reaction using alkaline catalysts. Therefore raw WCO is treated with the mineral acids ($HCl, H_2SO_4 and H_3PO_4$) for reducing its FFA contents [30]. In this work maximum reduction (75.6%) in the FFA was witnessed by treating the WCO with the H_2SO_4, this was then followed by the H_3PO_4 (62.9%) whereas minimum reduction (55.1%) was noticed with HCL.

FFA level was found up to 3.95 mg KOH/g in raw WCO. Such greater values for FFA is generally linked with longer chain molecules and reported not appropriate for transesterification reactions using the alkaline crystals. So the raw waste cooking oil was reacted with the mineral acids like (H_3PO_4, H_2SO_4 and HCL) for reducing the content of FFA [31]. In this work the minimum reduction (54.8%) in FFA contents was observed using HCL, followed by H_3PO_4 (62.9%) and the maximum reduction (74.8%) was observed when WCO was treated with H_2SO_4.

The key factor in the acid treatment was amount of methanol, as methanol concentration was increased the FFA reduced more efficiently. The other variables were temperature was 65oC, time for reaction was 200 min and the reaction speed was 600 rpm. The amount of methanol used in acid treatment was 2.25*FFA and sulphuric acid amount was 0.05*FFA. The FFA level was reduced in two steps. In first stage it was dropped from 4.05 to 1.5 $mg\ KOH/g$ and in the second stage it minimized to the level of $0.3369 mg KOH/g$. Hence after this procedure the WCO is transformed into the biodiesel using transesterification processing.

The quantity of catalyst used here was determined from Eq. (1)

$$\text{Catalyst amount} = \frac{Catalyst\ concentration \times amount\ of\ WCO\ used}{100} \quad (1)$$

There are five main factors which affect the biodiesel production are temperature, catalyst concentration, oil/methanol ratio, reaction time and reaction speed. To determine the optimal condition for biodiesel production a design project was utilized to plan experimental circumstances [32].

The biodiesel solubility in methanol was tested during biodiesel analysis [29,30]. Because triglycerides are insoluble while fatty acids methyl esters are (FAME's) are soluble in methanol [35].Methanol was mixed with WCO at a certain temperature (55–65 °C) in presence of KOH and reaction period (1–3 h) was permitted to settle down. Biodiesel appeared in top layer while glycerin was collected in bottom using the separating funnel. Biodiesel production was determined using Eq. (2)

$$Yield = \frac{Amount\ \ of\ \ biodiesel\ \ produced}{Amount\ \ of\ \ WCO\ \ used} \times 100 \tag{2}$$

Distilled water was used to wash the biodiesel and this method was repeated until distilled water came in transparent form.

The PH of biodiesel was measured using the *PH* measuring strips. The bomb-calorimeter(Oxygen) is utilized to find biodiesel calorific value [36]. The gas chromatographs and mass spectrum 5975C having triple I detector was used to determine the fame composition. Helium and Neon gases were used as carrier gases. To measure the acid value of waste cooking oil 50 ml distilled water was mixed with the 0.50 N KOH and this combination was used for titration. A blend of 30 ml alcohol and 0.30 g phenolphthalein was used as indicator. A mixture of 50 ml (5% distilled water and (95% ethyl alcohol) was prepared. Then 1 ml indicator was mixed with WCO solution. The acidic value of WCO is calculated using Eq. (3) and FFA value with Eq. (4)

$$AcidValue = \frac{56.1 \times V \times N}{W} \tag{3}$$

$$FFA = \frac{AcidValue}{2} \tag{4}$$

where V denotes the volume of distilled water used for titration and volume of KOH, N is normality of KOH and W represents to WCO weight.

The yield of biodiesel was optimized at optimal operating conditions. The level of FFAs in WCO was reduced using the acid treatment. Amongst all the mineral acids sulphuric acid H_2SO_4 was found very operative in reducing FFAs, it reduces FFAs up to 91.93%. WCO Transesterification with the methanol was found very effective, about 93.5% yield of biodiesel was produced with methanol/oil 8.60:1 ratio, 56.50 °C reaction temperature, 0.30% catalyst concentration, 610 rpm stirring speed and almost 3 h reaction period. Many physio-chemical properties explain the biodiesel quality. Oleic acid($C18:1$), Palmitic acid($C16:0$), α-linoleic acid($C18:3$) and linoleic acid($C18:2$) were main ingredients of biodiesel. Diesel engine performance characteristics were tested using diesel, B50 and B100 and compared.

2.2. Fuel sprays hydraulic characterization

The fuel mass flow (m) is basic parameter of the fuel injector-nozzle hydraulic characterization. This mass flow states total fuel mass which flows through a nozzle for interval of an injection event time (t) when indicator is in an open position. The injection factors will be pressure drop through orifice (P) that regulates velocity of flow through injector orifice. The entire mass flow can be easily determined by injecting a fuel into a container and measuring fuel mass injected for all the injections that is used to measure the mean fuel mass for all the injections. This process forms basis of simple trials to check the injector working in real world, like in the injector maintenance hall. This mass flow might explicate metering factors and may be valuable for the basic first law of thermodynamic examination however its use is bounded while considering the temporal spray advancement.

The mass flow rate of fuel or injection rate of fuel is critical in advancing the more comprehensive spray understanding and ignition process in the CI, spark ignition and gasoline engines. The hydraulic performance in the terms of injection rate regulator capability and fuel evaluating accuracy are absolutely a basic factor in the formation controlling, evolution and the combustion of spray. The GDI injector's introduction with the nozzle orifice modeled to affect the fuel sprays which interacts with the moving air happening in numerous areas of combustion cylinder which has led to requirements to take the complete understanding of mass flow rate of fuel through every orifice.

There are different approaches working to determine the injection mass flow rates. A mean flow rate $\dot{m}_{avg}$ can be measured from mass flow passing through injector nozzle and period of injection. The instantaneous flow rate $\dot{m}$ is time determined parameter of the mass flow rate which is very much valuable. Researchers used different approaches to determine the rate of mass flow during injection. Mainly two techniques are used to determine mass flow mate ($\dot{m}$) are Bosch method and Zeuch method [25,26].

Bosch method measures time determined $\dot{m}$ through measuring pressure variations through an injection event. In this method the fuel volume is injected into the length tubing holding the compressible fluid which generates the pressure wave, generally Diesel fuel. This injection produces a pressure variation which is measured to determine mass flow rate $\dot{m}$ using the scale. This method depends on the velocity–pressure equation, as this is applicable to single pressure wave in a moving flow [39].

The Zeuch technique measures pressure of a chamber having constant volume for the duration of an injection. The injection is performed into a closed and constant volume cylinder full of an injection fluid. Inside pressure of chamber before injection is kept constant. For the period of injection, the fuel volume (q) is injected into chamber which results in the pressure increase.

In previous researches different methods of measurement of mass flow injected through nozzle under a diesel engine alike situations was practiced by Nabers and Siebers [40]. Payri et al [41] and the Emberson et al. [42].

The average fuel mass flow rate is measured from fuel mass (m) injected by the nozzle and duration of injection. The measurement of mass of fuel injected is basically hydraulic characterization of fuel injection strategies and fuel types. Mass flow rate is definitely an important parameter in order to control the formation of spray. But it is crucial to gain a complete information of spray formation and combustion characteristics in compression ignition or in spark ignition engine. In

advance instantaneous mass flow rate ($\dot{m}$) that gives much more understanding as it is time resolved parameter.

The momentum flux of spray using impact force measurement is a recognized technique used for spray characterization. In this method momentum flux of emerging spray is measured by measuring the impact of spray. A Force sensor/transducer is positioned in front of an emerging spray from nozzle in such a way the measuring surface is at right angle to the spray axis. It is used to evaluate the both tip penetration and inside phenomena of nozzle orifice channels [43].

This phenomenon of control volume (CV) is show in Fig. 1as the spray is striking on target (see Fig. 2).

This measured force in actual represents the rate of momentum change as this rate of momentum change is equal to applied force. To govern the interaction of spray target following momentum conservation equations are used.

$$F = \frac{\partial}{\partial t}\int_{CV} \rho v dV + \int_{A} v^2 \rho dA \tag{5}$$

ρ and v and shows the density and velocity respectively in control volume (CV), dV shows differential of volume, dA shows differential area is taken as normal vector and F is a resultant force. On right side first term shows rate of momentum change stored by control volume (CV) and secondary term shows momentum flux $\dot{M}$ through a control volume. This equation is applied along the axis of spray and simplified by making some assumptions. The area through liquid jet is exiting is equal to geometrical area of orifice; the air along the axis of spray is negligible, hence speed of air is zero as

effect of gravity is negligible; fluid mass is negligible which is accelerating in control volume (CV) that makes first term of Eq. (5) zero; spray deviancy striking face of target is orthogonal to center axis of spray so fluid leaving the CV has no axial component of velocity; ρ_f is liquid density that is a constant value and liquid stream leaving to orifice(hole) has an uniform velocity (v_{eff}) [44]. The above made assumption concludes that the area through liquid jet is leaving to orifice is equivalent to geometrical area (A_{geo})of orifice shows that there is no cavitation present. Thus, only the second part of Eq. (5) gives the details of resultant force (F) striking on transducer face with axial liquid jet velocityv_{eff}. The force is equal to momentum flux leaving to orifice $F = \dot{M}$. Hence interaction faced by target is presented in form of

$$\dot{M} = \rho_f A_{geo} v_{eff}^2 \tag{6}$$

Eq. (6) shows that liquid jet velocity v_{eff} is directly proportional to the momentum flux square root $v_{eff} \propto \sqrt{\dot{M}}$ and instantaneous rate is given by.

$$\dot{m} = \rho_f A_{geo} v_{eff} \tag{7}$$

The above relation which shows that momentum flux square root $\dot{m} = \propto \sqrt{\dot{M}}$

Siebers and Nabers [40] propose that we can determine a relation among the instantaneous mass flow ($\dot{m}$) and momentum flux ($\dot{M}$) by normalizing transducer output square root through region under a curve for output square root $\int_0^t \sqrt{\dot{M}}.dt$. The result profile obtained from normalization is directly proportional to injection velocity that when multiplies with total mass of each injection yields instantaneous mass flow rate. Using Eqs. (6) and (7) normalization is conducted which yields the mass flow rate in the form of

$$\dot{m} = \sqrt{\dot{M}\rho_f A_{geo}} \tag{8}$$

During injection the total mass injected is given by

$$m = \int_0^t \dot{m}.dt = \int_0^t \sqrt{\dot{M}\rho_f A_{geo}}.dt \tag{9}$$

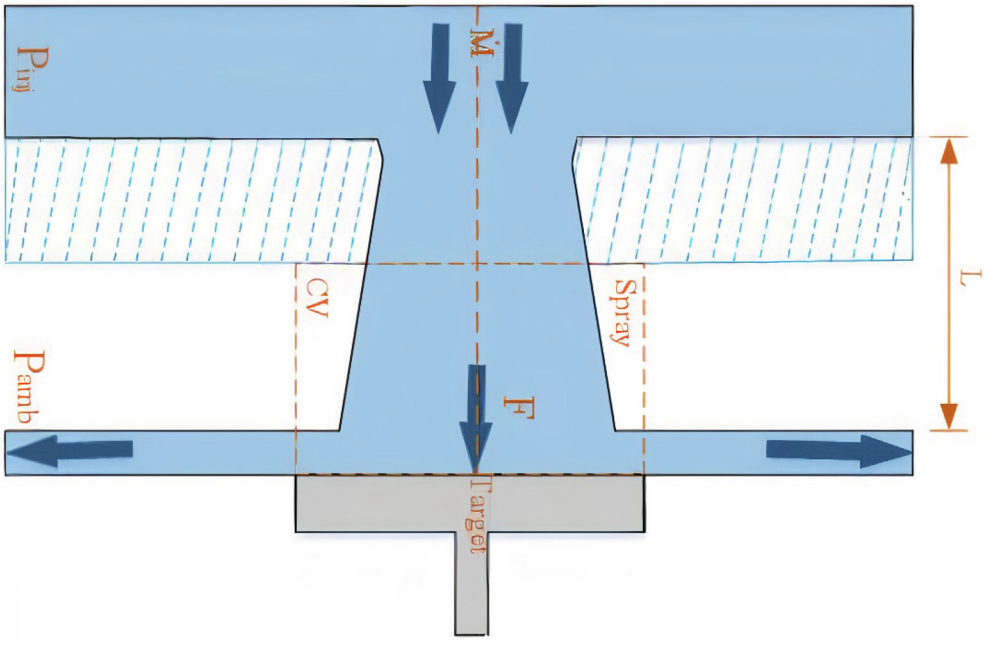

Fig. 1 Conceptual CV of emerging fuel spray developing from injector nozzle and striking to the target fitted with force transducer measuring sensor.CV = control volume, P_{inj} = injection pressure, P_{amb} = ambient pressure, F = force measured by sensor.

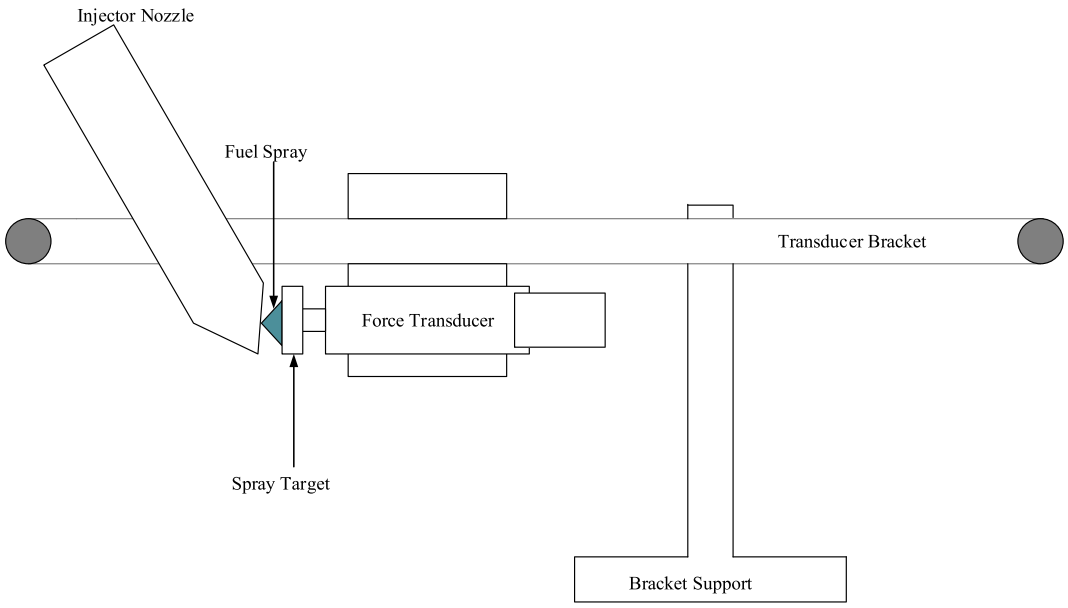

Fig. 2 Schematic drawing of force transducer attached with target placed in front of emerging spray.

The instantaneous mass flow rate is expressed as

$$\dot{m} = \frac{\sqrt{\dot{M}\rho_f A_{geo}}}{\int_0^t \sqrt{\dot{M}\rho_f A_{geo}}\ .dt} m = \frac{\sqrt{\dot{M}}}{\int_0^t \sqrt{\dot{M}}\ .dt} m \tag{10}$$

Density of fuel and instantaneous flow rate ($\dot{m}$) can be determined through momentum flux (Force transducer outturn) and entire fuel mass injected throughout injection process. The total fuel mass injected could be independently determined by accumulating the fuel during injections in fuel tank and weighing fuel mass to different injections. That method is used in many works [33,34].

The coefficient of discharge (C_d)is usually defined as a ratio of real flow rate passing from orifice to a theoretical flow rate passing from orifice for a single fluid and for similar pressure drop across orifice. It can be supposed of that as nozzle efficiency (on basis of mass flow) that portray the mas flux passing through orifice and might be determined by

$$C_d = \frac{\dot{m}}{\dot{m}_{th}} = \frac{\dot{m}}{A_{geo}\ \rho_f \upsilon_B} = \frac{\dot{m}}{A_{geo}\ \sqrt{\rho_f 2\Delta P}} \tag{11}$$

The discharge coefficient (C_d) can be splitted into two portions. Actual flow velocity can be lessened from maximum theoretical velocity (V_B) to υ_{eff} due to turbulence, friction and boundary layer special effects in injector orifice. So the reduction of velocity is determined from velocity coefficient which is described as

$$C_v = \frac{\upsilon_{eff}}{V_B} \tag{12}$$

Secondary part of $C_d$is measured by contraction area coefficient (C_a). This coefficient measures for losses of flow area due to cavitation, holes of outlet section and non-uniform velocity which results in the vapor bubbles [47]. To examineC_v, C_a and C_d of a nozzle momentum flux techniques have been utilized [48].

In literature cavitation number is defined in different forms but generally it is based on pressure variation across injector hole [49].A general form of cavitation number defined by [50].

$$K = \frac{P_{inj} - P_v}{P_{inj} - P_{amb}} = \frac{P_{inj} - P_v}{\Delta P} \tag{13}$$

At beginning of cavitation C_d reduces. Previous researches neglect vapor pressure because of their smaller size as compared to other pressures [51]. The cavitating flow passing through hole will decrease the cross-section area decreasing the coefficient of discharge. To perform any assessment the vapor phase is supposed as fixed and slip boundary that contains a fixed portion of orifice sector. Mostly this occurs at throat, close to the inlet of orifice as this is the point where liquid go through the most important direction change due to which velocity changes.

Hence discharge coefficient holds a direct proportional to square of cavitation number [51] as expressed in Eq. (14).

$$C_d = C_c\sqrt{K} \tag{14}$$

The value of k rises as back pressure rises or injection pressure reduces, with rise in k there is an instant where the cavitation vanishes and coefficient of discharge remains constant, this is named asK_{crit}. For higher values of K_{crit} flow would be completely in liquid stage and reliant on the Reynolds number [48].

The graph of cavitation number square root and discharge coefficient measured using momentum flux is utilized to observe the nozzle cavitation and marks the fluid state or injection pressure where cavitation starts [52].

2.3. Experimentation

A common rail (CR) system was utilized to deliver fuel to the injector at high pressure. The system was constituted through a pump driven by compressed air which can supply the fuel up to

250 MPa. A force transducer having a force measurement range of $(0-10N)$was needed to determine the spray effect. It needed a device having risen time in microseconds ($<10us$) because of short period measurement scale. This narrow time measurement scale and oscillatory nature needed a device having minimum natural frequency of 50 KHz [53]. The force transducer face which is placed in front of high-pressure impinging spray should be resilient to the chemical erosion.

The injector used was piezo-actuated Siemen minisac type havig seven holes. Because of the nozzle orifices arrangement, it was compulsory to block the all holes except on orifice to allow the single spray observation and examination. All the orifices were blocked through laser welding with the jewelers welding outfit. The pressure transducer was fixed in the rail to measure the common rail pressure and it was taken to injection pressure.

The force transducer (Kistler model 9215) was selected for this work already has been used in different works [41–43] The piezoelectric force transducer used to measure dynamic and quasi-static forces (tension & compression) from (20–200 N) with capability to measure weight upto 1mN. The transducer contains sensor body having outer threads for holding the transducer with clamp. The front face contains a 2.5mm threaded hole to receive a threaded screw. The screw transferred force to transducer's sensing part. In actual the screw head was dome shaped. This dome-shaped screw was swapped with a plane surface steel screw having 5 mm diameter. This screw was placed in front of fuel spray. As the spray is striking on target, this force is equivalent to momentum flux at that cross section.

A high pressurized chamber is used for all the injections [56]. The chamber was completely filled with the nitrogen at the pressure of 20 and 30 bars related to their ambient densities of $22.7kg/m^3$ and $34.6kg/m^3$ correspondingly at ambient temperature of 20 °C. At this pressure we can get the density level normally occurred in diesel engines at the time of injection (10–40 kg/m^3). The force transducer was placed in front of injector-nozzle with the help of an iron bracket linked to a supporting rod which in advance was fixed to chamber base see Fig. 5. The injector orifice center axis relative to injector body center axis was determined by silicon mold of injector orifice a technique used in previous work.

The design of bracket permitted the force transducer target gap from injector to be calibrated. During all measurements here the space between transducer and nozzle was kept to least to 0.5 mm due to injector geometry. The other distances used previously were in the range of (0.5–10 mm) [45–47]. The transducer was positioned using the feeler gauge. The previous work [60] showed very small variation in momentum flux calculated for different distance ranges but their results examination showed that smaller value of 0.5mm gives better results. Once transducer and bracket are fixed in a position were not allowed to move in any direction during collection of data phase. Good calibration was strived and desired for but slight fluctuations in angle by ideal arrangement are unavoidable. This error is very minor as force(F) is linearly proportional to $cos(\Delta\theta)$ and θ is the divergence from ideal arrangement, for smaller angles $cos\theta$ is almost 1

The force transducer signals were amplified using a charge amplifier (Model 5007) [49,50].The voltage signals at output were acquired using charge amplifier at the frequency of 90KHz bthrough DAQ card. Injection mechanism was controlled by custom Lab-view database which also controlled data collection. The data acquisition contained voltage signal that was directly related to force applied on the target by fuel spray.

A common rail injection setup using the high-pressure BOSCH CP1 volumetric pump run by a 56kw electric driven motor, and an ordinary common rail system fitted with piezo force sensor was used. The Siemens, mini sac, piezoelectric injector was used with 120 um diameter, 7 holes and is handled by the Hartridge driver. Piezo injectors use results in a precise timing of open and close power exerted to needle, having decreased transient time in calculated momentum flux. It has progressive influence on the spray target interface at beginning of injection.

The nozzle conicity $(k-factor)$ is defined by $K=\frac{D_i-D_o}{10}$

The k-factor of injector-nozzle was calculated using calculations made in scanning electron microscope (SEM) from silicon mold of injector geometry, as given in Table 1. The inner radius of orifice was also measured by SEM and was estimated to nearly $69.5\mu m$. The recording of data began with TTL trigger that was directed to the Hartridge driver. The duration of Injection for all assessments was fixed to 0.4ms (TTL timing0.4ms). The injection pressures 600, 800 and 1000 bar were taken. Before placing in chamber transducer was regulated through known masses between $40-200g$ (around 0.4–2 N). For each load 10 evaluations were taken to build a strong calibration contour to inspect the linearity above range. Then gradient of the calibration line was established as calibration persistent to extract the force through voltage signals recorded by LabView.

For every assessment a total number of 120 injections were taken having an interval of 1s between every injection. The signals recorded by LabView were scaled to measure the force through calibration persistent.

All fuels utilized in this research were characterized by density(ρ) and viscosity(μ). The density of fuel was determined by 10ml scaled beaker and scales set (OA-AV114). All measurements were repeated 12 times taking same scaled cylinder. Viscosity of the fuel was measured using the TA instrument (AR 2000 rheomoter) and shear rates were adjusted spontaneously using rheometer from $(20-1000S^{-1})$.

For absolute hydraulic characterization complete fuel injected mass should be known. To achieve this the fuel was injected into a flask with an adaptable lid. After the 600 injections flask was weighted on a weighting scale (AV114). So the average fuel mass injected/injection was computed. This procedure was reiterated five times for every situation. The instantaneous $\dot{m}$ was measured using average, scaled momentum flux results and total injected mass from Eq. (10).

3. Results and discussion

3.1. Momentum flux of fuel sprays

The momentary variation of $\dot{M}$ over whole injection duration for the diesel, B50 and B100 is shown in Fig. 3 for almost all

Table 1 Physical properties of diesel, B50 and B100.

No.	Properties	Diesel	B100	B50
1	Density at25°C(kg/m^3)	831	892	859.5
2	Viscosity at35°C(mm^2/s)	3.9016	5.69	4.933
3	Acid value(mgKOH/g)	0.247	0.6732	0.285
4	Flash point (℃)	79	140	120
5	Pour point (℃)	7	1.2	3

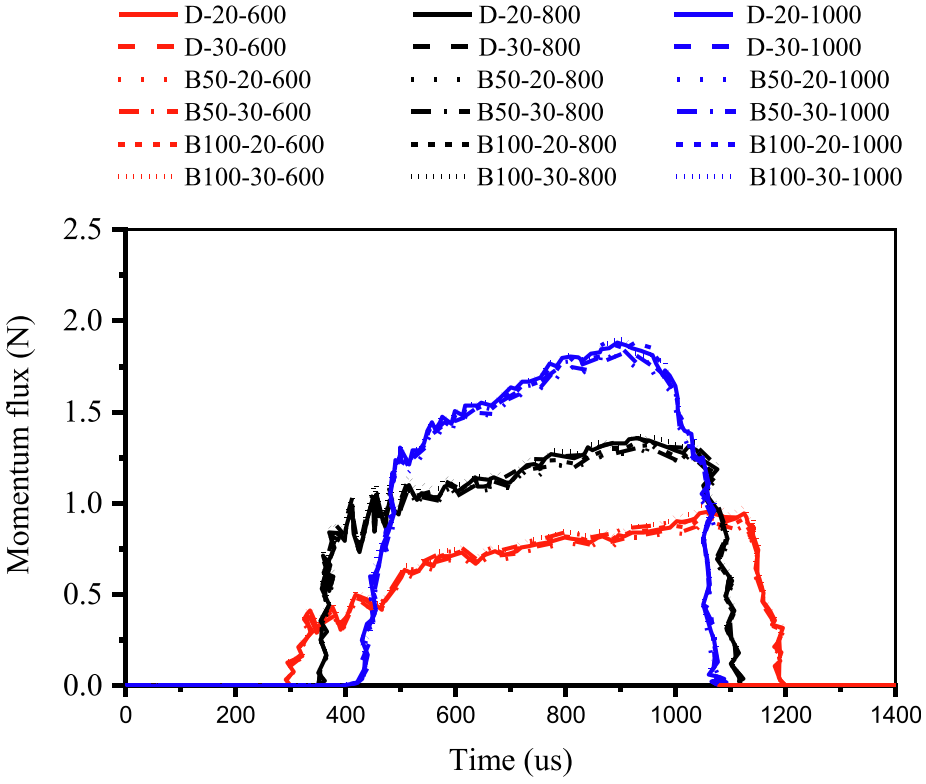

Fig. 3 variations in the momentum flux of fuel spray with timet, after data collection starts (without removing the injection delay period) for Diesel, B50 and B100 at P_{inj} = 600 (red), 800 (black) and 1000 bar (blue) $\rho_a = 22.7 Kg/m^3 (P_{amb}$ = 20 bar). $\rho_a = 34.6 Kg/m^3 (P_{amb}$ = 30 bar).

conditions of injections. The arc shows arithmetic mean (A.M) $\dot{M}$ of 120 injections for all conditions. No lumps have been eliminated for signal smoothing. A testing scale of 100 KHz (Sample through 10μs) has been used. In this graph no adjustment to eliminate the injection delay period has been made.

The time interval between injections being commenced through controlled software (TTL-signals received by driver from the Pc) and staring of spray is defined as injection delay or injection retard. The injection delay is comprises of a micro-electronic fraction from control mechanism, especially hydraulic fraction and the injector driver that appears due to higher pressure of fuel acting on several valves and on the inner surfaces of injector body. The fraction of injection delay which has been named as ''electronic delay period'' is supposed to a constant value for all operating situations and is neglected from now on. Variance in the injection delay period is shown by change in time, t while $\dot{M} > 0$ is completely from variant in hydraulic delay period. As injection pressure rises from 600 to 800 and 1000 bars it results increase in injection delay period from 305 to 340 to 390 μs correspondingly. At end of the injection, it is very difficult to qualify such as computed momentum flux $\dot{M}$ does not shows the same fall to zero as it rises from zero at SOI.

The EOI take place earlier approximately at 1200, 1160 and 1120 μs as injection pressure rises from 600 to 800 to 1000 bar. At EOI the hydraulic delay is reflection of SOI, leading to drop in actual injection duration with rise in injection pressure. Injection period consumed here is very small as a 0.5 ms TTL signal sent to driver of injector. In actual injection the effective interval is 895, 820 and 730 μs for injection pressures 600, 800 and 1000 bar respectively. B50 and B100 had no significant effect on the injection duration and delay.

In actual hydraulic delay depends on design of injector. The injector type used here is indirect and electric-hydraulic servo using an unstable control valve [63]. A piezoelectric actuator runs the mushroom valve inside injector's-controlled chamber. After actuated, valve opens and allows higher pressure fuel to come in the controlled chamber and discarded out of the fuel to injector back port. The decrease in pressure of controlled chamber permits the needle indicator to thrill up to open the nozzle. Mushroom valve was kept closed using a spring-helix and a fuel pressure system. An increment in the injection pressure results in the greater force and will keep mushroom valve closed. Here increment in time will take for opening of mushroom valve after piezo is activated. This is consequence of such kind of injector design [64].

In Figs. 4 and 5 transient variance of momentum flux ($\dot{M}$) over complete injection duration for the Diesel, B50 and B100 injection sprays at ambient densities of $22.7 kg/m^3$ and $34.6 Kg/m^3$ respectively is shown. The initially non-zero measurements of $\dot{M}$ are utilized to inline SOI for every situation so to make a comparison amongst all cases when hydraulic delay period is removed. Hence SOI for every condition has been fixed at t-50μs. For every case initial rise in the $\dot{M}$ is very hasty as the spray leaves injector and raids at face of transducer target. Hence $\dot{M}$ rises very rapidly during initial period (100-200μs after the SOI) in Figs. 4 and 5 when a high injection pressure is applied.

For whole duration of injection, the greater injection pressure generates greater$\dot{M}$. In the early 50μs there is significant overlap of the $\dot{M}$ trend-lines which makes difficult to illustrate any ambient density or injection pressure effects. After almost 100 μs gradient of curve reduces for all the cases and variance in momentum flux almost looks linear until it reaches to peak value of momentum flux. After SOI around 100μs the $\dot{M}$ of injections at ambient density 22.7 kg/m^3 increases in size as compared to 34.6 kg/m^3 curves.

The initial phase of injection shows variation on a larger scale in average $\dot{M}$ signal as shown in figures. This is due to quick transients in spray formation that can be named as the hydraulic noise. While curves in Figs. 4 and 5 are compared for similar injection pressure this shows a decent alignment between hydraulic noises that recommends these noises are repeatable and the injector-nozzle feature and forces transducer target collaboration at these circumstances (ρ_a, P_{inj}, fuel kind, injector stimulating time period).

The highest 10 values near peak value of $\dot{M}$ are utilized to find an average $\dot{M}$ peak value for every condition($\dot{M}_{mean}$). This average peak value $\dot{M}_{mean}$ is an illustrative value for every testing condition and this is used to build the Fig. 6. During primary testing the momentum flux was also collected for longer injection duration of 2 ms. It was experienced that using maximum ten(10) assessments for each 0.5ms injections are an appropriate way to represent a value for every condition. The direct relation between measured momentum flux $\dot{M}$ and applied injection pressure is demonstrated.

The upper broken(dashed) blue trend line on graph is fitted to points of injections collected at the density(ρ_a) of $22.7 kg/m^3$ .The lower blue broken(dashed) trend line on plot is fixed to the points of injections collected at ambient density ρ_a of $34.6 kg/m^3$. By changing ambient densities pressure drop also changes across the nozzle as densities were changed through changing the chamber pressure. The theory discussed in the Section 2.2 and presented in the previous works [53,54] proposes that $\dot{M}$ determined in this mode would not be affected by atmospheric densities at which injection is occurring. If this case was realistic and $\dot{M}$ was simply reliant on ΔPthrough nozzle then it should expect all spots to exist on a same track.

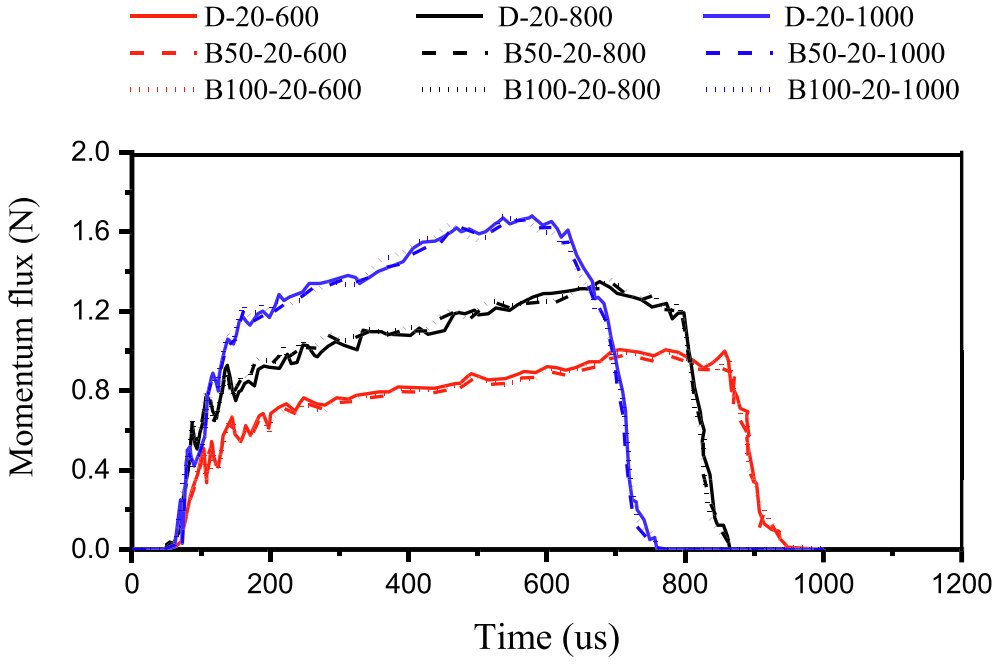

Fig. 4 Variation in momentum flux of fuel spray against time t, for Diesel, B50 and B100 fuels. P_{inj}(bar) = 600(red), 800(black) and 1000(blue) $\rho_a = 22.7 Kg/m^3$ (P_{amb} = 20 bar).

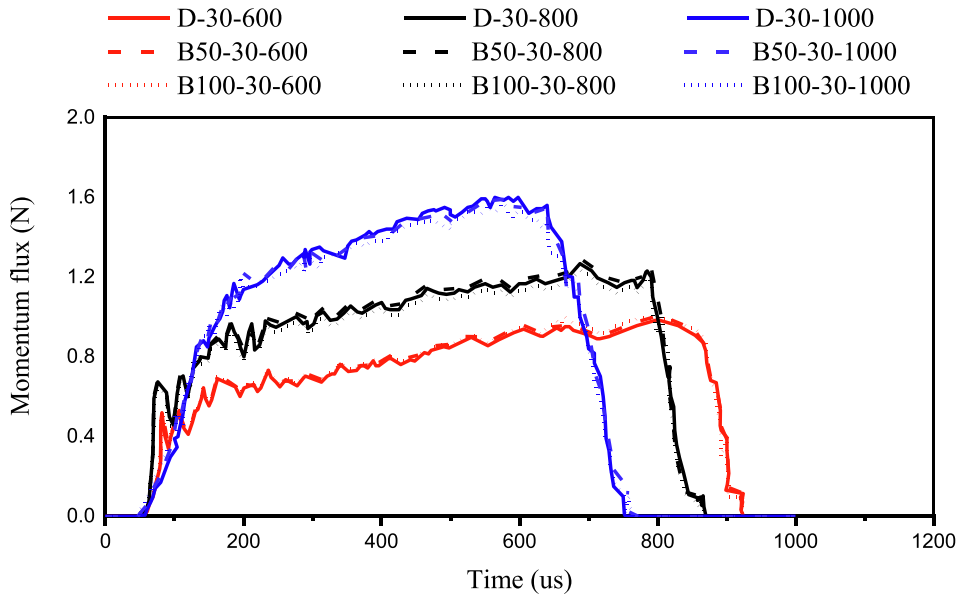

Fig. 5 Variation in momentum flux of fuel spray against time t, for Diesel, B50 and B100 fuels. P_{inj}(bar) = 600(red), 800(black) and 1000(blue) $\rho_a = 34.6 Kg/m^3$ (P_{amb} = 30 bar).

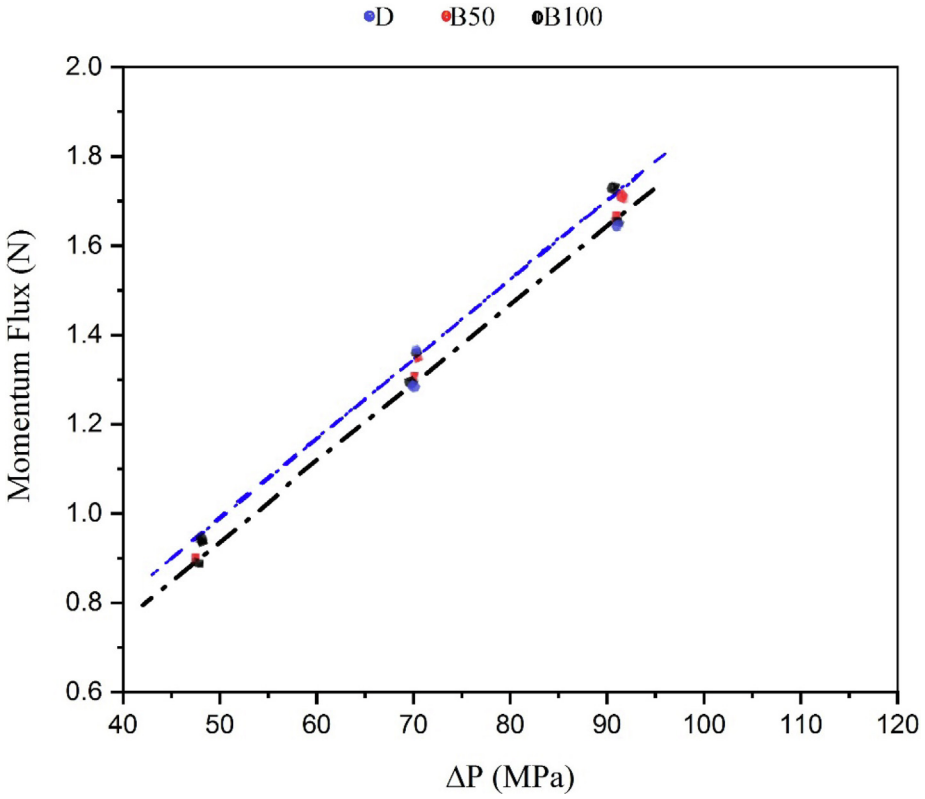

Fig. 6 Momentum flux mean peak value for Diesel fuel(blue), B50(red) and B100(black) against pressure drop (ΔP)across an injector nozzle. The blue dashed line represents injections with $\rho_a = 22.7 Kg/m^3$(P_{amb} = 20 bar). The black dashed line represents the injections with $\rho_a = 34.6 Kg/m^3$(P_{amb} = 30 bar).

Even though effect is minor, the higher number of test groups recommends the significant difference. The $\dot{M}$ was measured at 0.5 mm from nozzle outlet. It was never estimated that $\dot{M}$ measured at this closeness from nozzle exit will show variations at different ambient densities as major part of spray at this range comprise of liquid state which had very small interaction with gas. Results obtained here commend that the liquid core spray leaving to nozzle is experiencing an

exchange in momentum with change in surrounding gas density even at the space of 0.5 mm from nozzle outlet. For every condition diesel, B50 and B100 had small to no influence in average peak $\dot{M}$.

3.2. Total mass injected:

The Table 2 given below shows average fuel mass injected for every single fuel at every pressure measured through 5 sets of 600 injections. To determine the repeatability amongst all five(5) cases relative standard-deviation(σ) is induced. As revealed, the momentum flux $\dot{M}$ depends on ambient densities of surrounding. It will be workable to suppose that ambient densities might have influence on injected mass that, considering entire masses achieved at ambient **circumstances is not taken here (see Table 3).

The statistics from Table 3 have been displayed in Fig. 7. For every condition the diesel fuel mass injected is greater than both B50 and B100 for every injection pressure. Both B50 and B100 shows a similar value of injected mass. Variance between the diesel, B50 and B100 is almost have a same value for every injection pressure.

3.3. Fuel viscosity and densities

The viscosity and density for all fuels have also been calculated. For every case the viscosity showed a constant value when value of shear-rate(γ) was in between 420 and 1050s^{-1}. The average value shown is calculated by taking the average of this constant duration. The measurements were repeated 3-times to obtain a mean value of viscosity for each fuel.

The B50 and B100 showed a slight increment in density of fuel. This is predictable because of biodiesel addition which has greater density than simple diesel fuel. These measured densities have been compared to ideal mixture density. This ideal mixture can be stated with respect to two dissimilar mixtures of model. One depends on supposition that mass is proportional to volume of solution and uses fraction of mass and densities for every substance.

$$\rho_n = \sum (x_i p_i) n \tag{15}$$

Mass fraction is denoted byx_i. The next method supposes that additive volumes can be more suitable for immiscible fluids like diesel fuel and water.

$$1/\rho_n = \sum (x_i/p_i) n \tag{16}$$

In Fig. 8 the measured results and analytical models are presented. The computed density for B50 is almost same to the predictive models. While the density measured for B100 is much greater than is expected by both mixing models. So, this proposes that for diesel blends as biodiesel is added more phases become dispersed and larger and drops may compact more close to each other leading to increment in the density.

A slight increment in density of B50 and B100 might be expected to rise in fuel injected mass taking injected mass as$A_{geo}\sqrt{\rho_f 2\Delta P}$.

That was not which is observed in Fig. 7.The addition of biodiesel results an increment in calculated viscosity as compared to simple diesel fuel. This rise in the viscosity would be opposing increment in fuels densities to lower fuels injected mass during opening time of needle.

3.4. Instantaneous mass flow rate

From Eq. (10) transient $\dot{M}$ and total fuel mass injected independently measured the transitory instantaneous flow rate $\dot{m}$ has been calculated for each condition. The integral of momentum flux square root in Eq. (10) is defined by are under the curve $\dot{M}$ and calculated mathematically with trapezium method in the Matlab. Transient profile $\dot{m}$ example is shown in Fig. 9. This contains profile for every fuel at every injection pressure at densityρ_a = 22.7 kg/m^3.

The total injected mass is different for every fuel which changes the $\dot{m}$ for B50 and B100 when compared to simple diesel. The leading 10 readings of $\dot{m}$ for every case have been utilized to gain an average-peak outcome in a similar way as $\dot{M}$ average-peak value was calculated. $\dot{M}$ average peak value in Fig. 6.

For every condition the average peak values used as illustrative value of $\dot{m}$ has been utilized to form Fig. 10. The linear relation of $\dot{m}$ with pressure drop square root across injector nozzle is established. Both B50 and B100 shows a similar peak value of $\dot{m}$ at every injection pressure. When injection pressure rises difference among clean diesel, B50 and B100 gets bigger. The average-peak value of $\dot{m}$ is almost similar for every fuel at 500*bar* injection pressure. A difference of almost 0.3mg/ms at 1000 bar injection pressure is appeared. Although this difference is very minor, but it reflects mass scales and small interval scales which are engaged in measurement of all injection events. Instantaneous flow rate $\dot{m}$ difference between the B50, B100 and neat diesel fuel will be predicted while difference in entire injected mass is inspected in Fig. 7. This method may be accounted effective in producing instantaneous mass flow rate plot which can be utilized as an input in multidimensional engines.

Table 2 K-factor and injector nozzle diameters.

$D_{inlet}(\mu m)$	$D_{outlet}(\mu m)$	K factor(μm)
139	119	2

Table 3 Fuel mass injected in each injection for Diesel, B50 and B100.

Fuels	Injection pressure (bar)	Fuel mass injected (g)	Relative (σ) (%)
Diesel	600	0.002357	0.2
	800	0.002670	0.4
	1000	0.002762	0.8
B50	600	0.002289	0.9
	800	0.002592	0.6
	1000	0.002678	1
B100	600	0.002265	0.6
	800	0.002496	0.7
	1000	0.002682	1.9

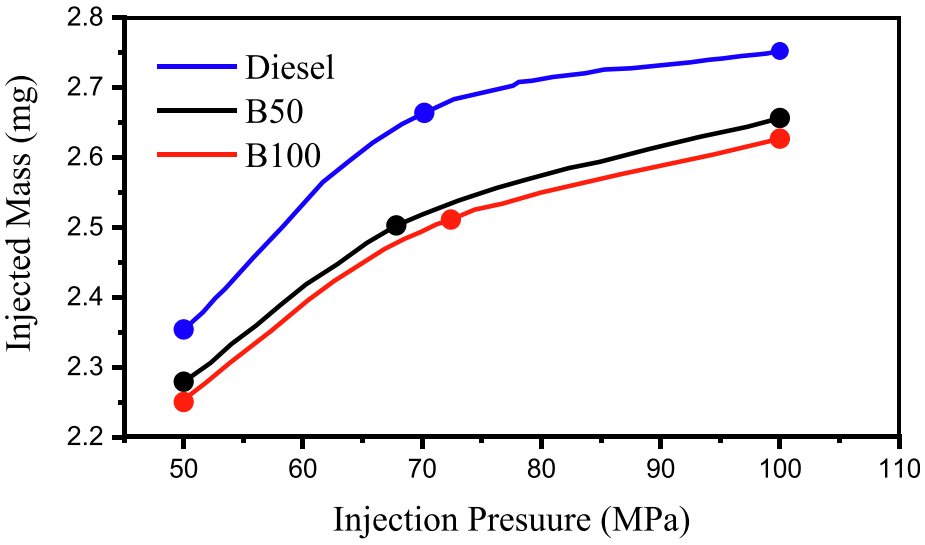

Fig. 7 Total injected mass for Diesel fuel(blue), B50(red) and B100(black) at P_{inj} = 600, 800 and 1000 bar.

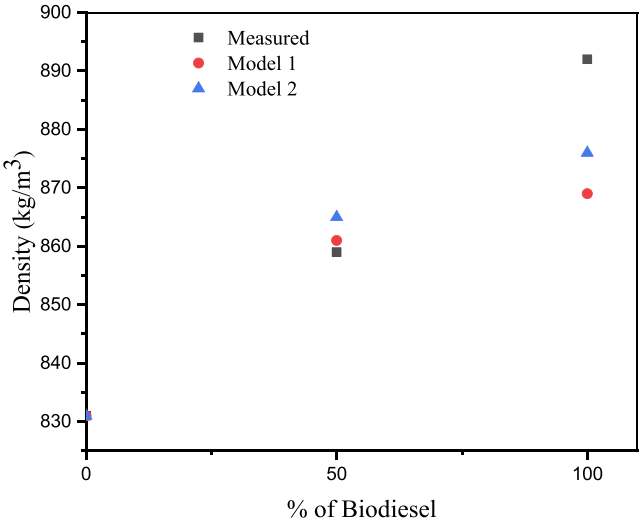

Fig. 8 Fuels density against % of biodiesel mixed. Densities determined using measurements in black, densities calculated from Eq. (15) in Red. Densities calculated from Eq. (16) in Blue.

3.5. Discharge coefficient

This coefficient(C_d) has been calculated using the Eq. (11) with$\dot{m}$. Cross section area(A_{geo}) of the injector nozzle orifice was measured using silicon mold of injector nozzle; injection pressure and fuel density.

The Fig. 11 shows cavitation number square root with C_d for every condition, as the injection pressure rises cavitation number decreases. The arrow direction in Fig. 11 shows an increment in the injection pressure. B50 and B100 have led to decrement in discharge coefficient of nozzle as equated with clean diesel results. It is clear that C_d does not change with varying injection pressure; hence it shows no indication that injector-nozzle is taking cavitation at any condition or K_{crit} has detected.

It is detected that coefficient of discharge changes slightly with changing k for each condition of fuel. The mixing process reduces discharge coefficients have not persuaded any cavitation formation at all injection circumstances. At injection pressure of 1000 bar ($\sqrt{K}$ is lower) difference in discharge coefficient C_d between neat diesel and B50 and B100 is considerable. The values of k observed in this work are limited in range as compared to other work which practice this analysis [67]. So, we can't access the condition at which cavitation started. This theory describes that flow depends on the Reynold number according to non cavitating conditions [68]. To observe the Reynold number behavior the mean velocity of flow is necessary along fluid viscosity and density. Characteristic length L_c applied is mean diameter of nozzle calculated from measurements given in Table 2 K-factor and injector nozzle diameters to be 130μs. The injection average velocity is determined using average-peak $\dot{M}$ and average-peak instantaneous rate ($\dot{m}$) values to form the Fig. 12.

$$V_{eff,mean} = \frac{\dot{M}_{mean}}{\dot{m}_{mean}} \tag{17}$$

The measured $\dot{M}$was nearly same at every condition for all fuels. The $\dot{m}$ for B50 and B100 was reduced than clean diesel fuel. The higher velocity of B50 and B100 maintain the momentum to almost a constant value. This is shown in Fig. 12 which reflects that as the injection pressure rises average injection rate of B50 and B100 was greater as compared to clean diesel. Injection velocity at 22.7 kg/m^3 was greater as compared with ambient density of 34.6 kg/m^3 for all conditions.

According to Eq. (18) of Reynold number the larger density and higher velocity of B50 and B100 will increase the Reynold number value whilst increment in viscosity of B50 and B100 results in decrement in Reynold number value. The range of Reynold number 4700–7400 within the fuels spray fall for all conditions. Considering larger scale for Reynold number measurement the difference between fuels Reynold number is very small. This proposes that, although cavitation is zero, but it

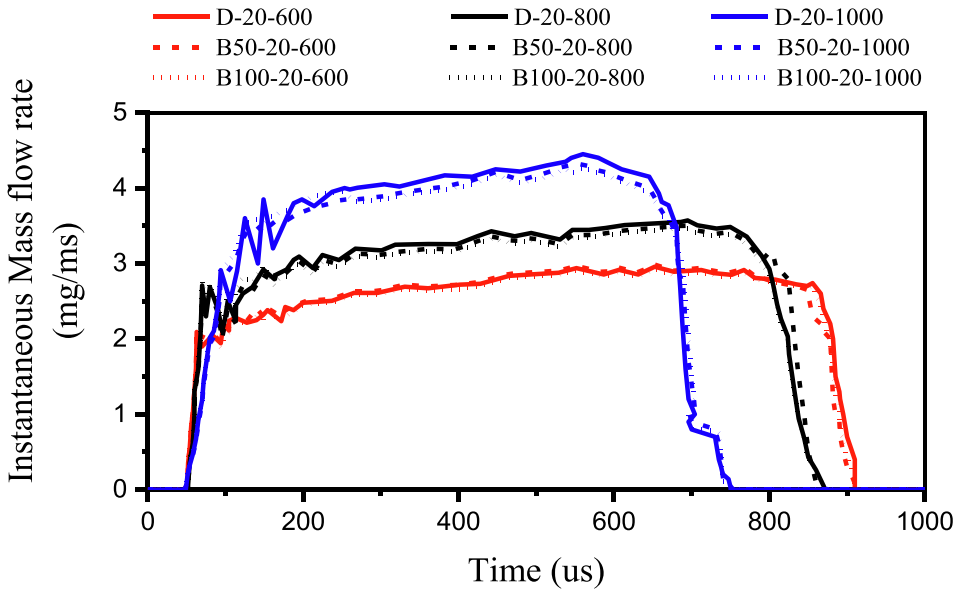

Fig. 9 Instantaneous ṁ profile against time t, for the Diesel fuel(solid line), B50(fine dashed line) and B100(course dashed line). P_{inj}(bar) = 500(red), 700(black) and 1000 (blue) $\rho_a = 22.7 Kg/m^3$(P_{amb} = 20 bar).

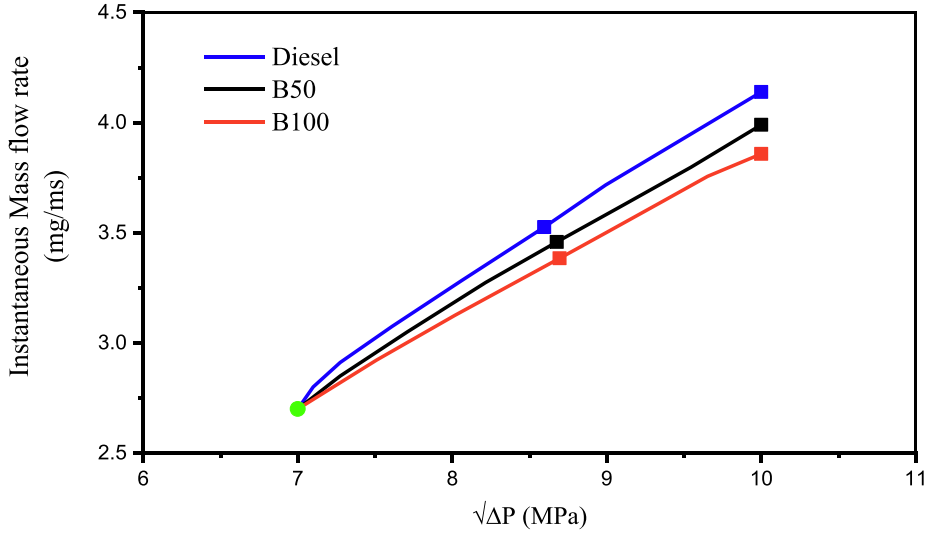

Fig. 10 Instantaneous ṁ average-peak value for diesel(blue), B50(red) and B100(black) fuels against $\left(\sqrt{\Delta P}\right)$across the nozzle.$\rho_a = 22.7 kg/m^3$ (P_{amb} = 20 bar).

may not the flow Reynold number in nozzle that is lowering discharge coefficient of B50 and B100. It is precious noting that values of Reynold number calculated in this work are lower than calculated than in previous work. This is understood because of very high viscosity determined here as compared with dynamic viscosity values in 0.0020*pa.s* range [57,58] that are frequently used.

$$Re_l = \frac{\upsilon D \rho_l}{\mu_l} \tag{18}$$

3.6. Momentum coefficient (C_m)

Whilst coefficient of discharge might be a key factor from the fuel metering opinion, spray momentum denotes the available energy to spray as this conserve momentum energy with surrounding gases. There are two momentum-based coefficients are announced here. One of them is named as momentum coefficient (C_m) [71]. Momentum coefficient is similar to discharge coefficient, defined as the ratio of momentum measured to theoretical momentum of fuel spray Eq. (19).

$$C_{Mmean} = \frac{\dot{M}_{mean}}{A_{geo}\rho_f \upsilon_{eff}^2} = \frac{\dot{M}_{mean}}{2A_{geo}\Delta p} \tag{19}$$

The representative momentum flux $\dot{M}$ average-peak values calculated in the Section 3.1 are utilized to find momentum coefficient(C_M). Change in mean Momentum coefficient (C_{Mmean}) with ΔP across nozzle is displayed in Fig. 13. The Increase in pressure drop(ΔP) increases theoretic momentum

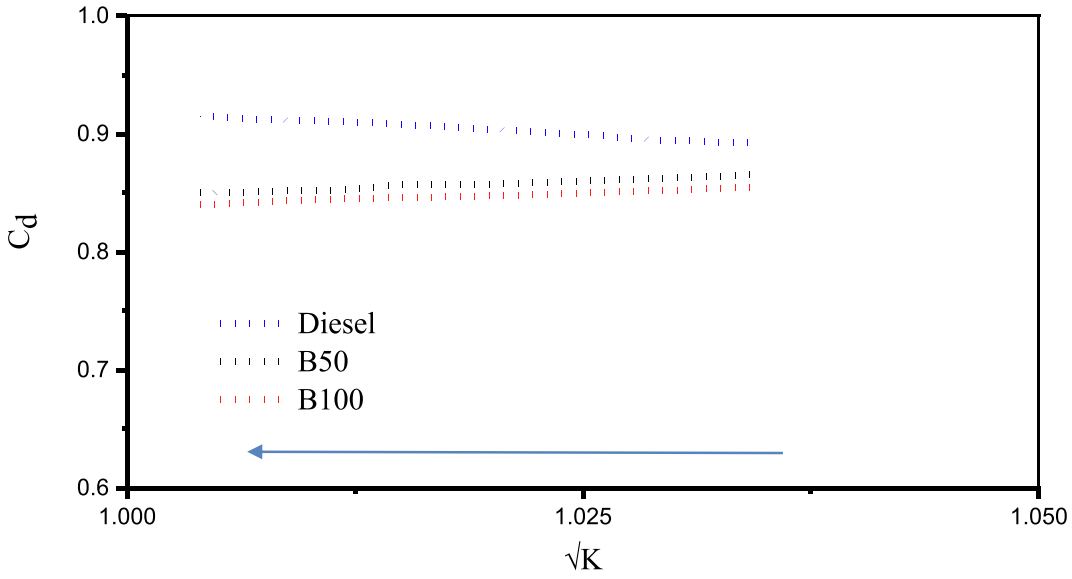

Fig. 11 discharge coefficient(C_d) of nozzle against cavitation number square root of Eq. (13) for Diesel fuel(blue), B50(red) and B100 (black).

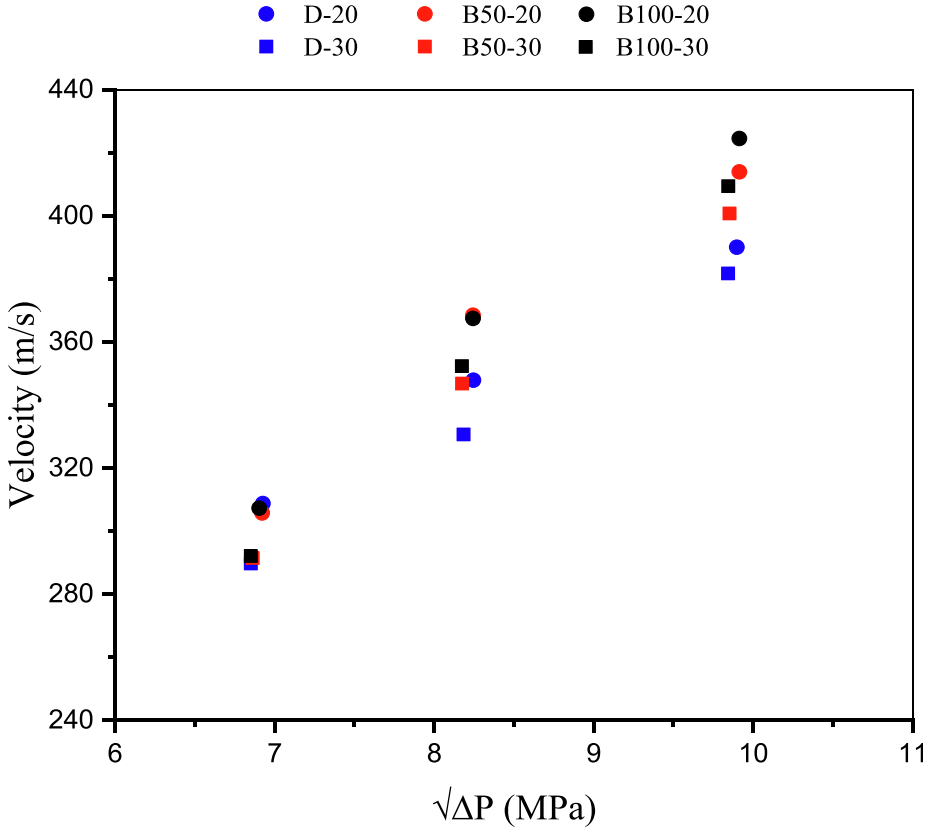

Fig. 12 Average(mean) peak injection velocity value for diesel fuel(blue), B50(red) and B100(black) fuels against ($\sqrt{\Delta P}$) across nozzle. .$\rho_a = 22.7 kg/m^3$ (P_{amb} = 20 bar) round circles. $\rho_a = 34.6 kg/m^3$ (P_{amb} = 30 bar) squares.

flux value of spray, results displayed in Fig. 6 also supports this declaration, however this is just after the coefficient of momentum is calculated which is clear and distinct that, in momentum terms, injector nozzle was not executing as have to be estimated by rising injection pressure. Hence for each fuel increment in ambient density inside chamber; caused a decrease in momentum coefficient. For all fuels at every injection condition the B50 and B100 had no significant influence on the momentum coefficient having identical almost very similar momentum coefficient.

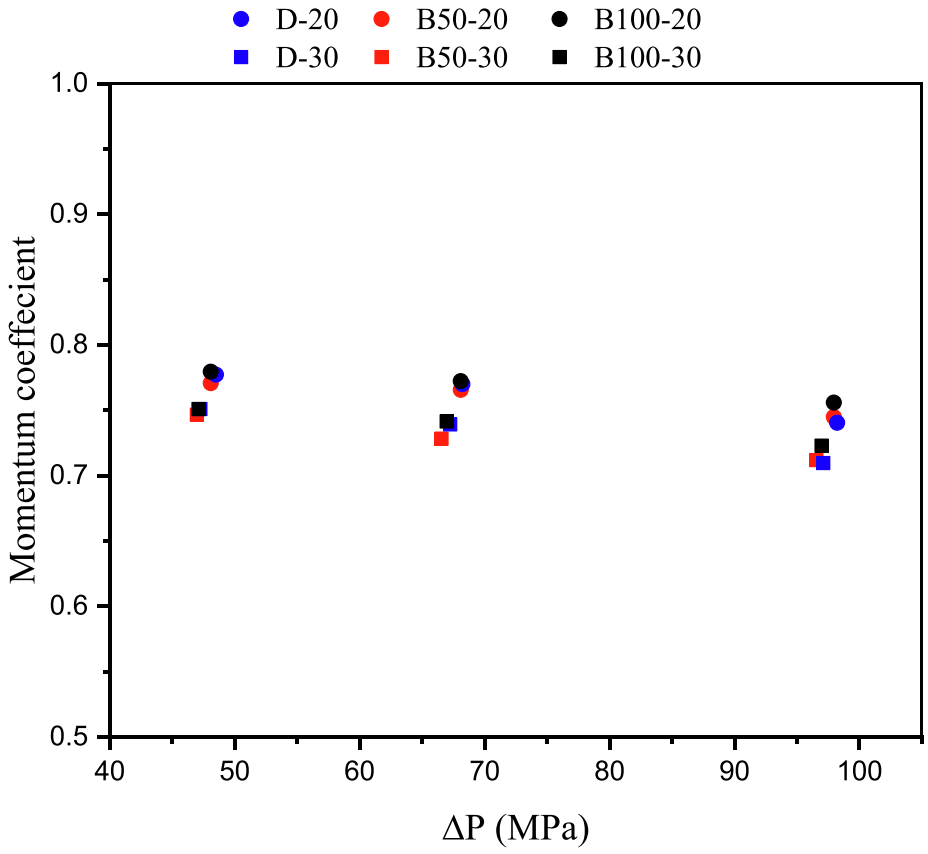

Fig. 13 Momentum coefficient (Eq. (19)) of fuel sprays for the Diesel(blue), B50(red) and B100(black) againstΔP across nozzle $\rho_a = 22.7\text{kg/m}^3$ (P_{amb} = 20 bar) round circles. $\rho_a = 34.6\text{kg/m}^3$ (P_{amb} = 30 bar) solid squares.

C_m has been determined using theoretical values of momentum flux($\dot{M}$) for every condition given as$2A_{geo}\Delta P$. Injector nozzle orifice geometrical area(A_{geo}) is being used again (that is established on assumptions previously defined) and it can declare a misinterpretation of effects on spray momentum. Instantaneous rates($\dot{m}$) have been calculated using the normalized $\dot{M}$ measurement technique and total injected mass. A single variation in fluids flow cross-sectional area through nozzle away from geometric area(A_{geo}) have been taken in for the measurement. So it would be appropriate to use computed mass flow by way of

$$\dot{M} = \dot{m}\upsilon_B \tag{20}$$

where υ_B represents the theoretical velocity which is used to calculate momentum efficiency.

$$\eta_m = \frac{\dot{M}}{\dot{m}.\sqrt{\frac{2\Delta P}{\rho_f}}} \tag{21}$$

This separates all effects of area contraction of cavitation and accounts only nozzle orifice losses due to velocity variations. In Fig. 14 momentum efficiency of nozzle for every fuel is presented. The clean diesel fuel shows a linear reduction in momentum efficiency as injection pressure increases that is larger than decrease for B50 and B100. The higher density of chamber leads to decrease in the momentum efficiency (η_m) for every fuel at every injection pressure. The B100 fuel has largest momentum efficiency (η_m) at every condition, following by B50 with clean diesel displaying the lowest efficiency at every condition. The B50 and B100 presented here leads to an increment in injection velocity as compared to clean diesel. Hence this is a counter increment in viscosity which rises due to blending process that can be expected to minimize flow velocity.

The complicated type of multi axis flow has not freely described with calculations in this section. It is clear that large viscosity that would be estimated to minimize velocity of flow is not a single technique working on B50 and B100 as they injected. This is uncertain that in which way B50 and B100′s viscosity and density go as injection is exposed to a high pressure. The higher pressure drop (ΔP) linked with radical variation of fluid path as fuel leaves injector can outcome in formation of smaller viscosity area in nozzle from which fuel can flow with greater velocity.

3.7. Summary and conclusion

$\dot{M}$ of fuel sprays; Diesel and B50 then diesel and B100 has been analyzed using a kistler model force sensing transducer positioned at a space of (0.5mm) from injector nozzle exit point. Every injection has been conducted at injection pressures of 60, 80, and 100Mpa into a high-pressure nitrogen filled chamber having back pressures of 20 bar and 30 bar producing an inside chamber density of 22.7 and 34.6kg/m^3 respectively. Spray period was small at 500μs however it had been established that during this period the fuel spray reached to a sensi-

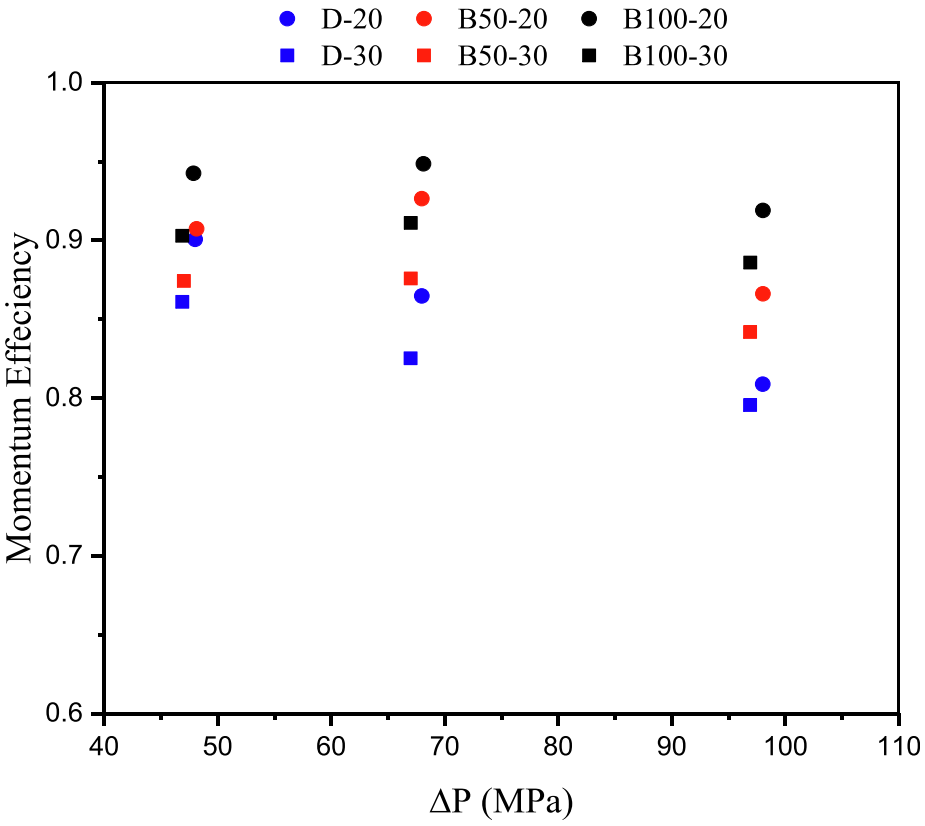

Fig. 14 Momentum efficiency (Eq. (21)) of fuel sprays, Diesel(blue), B50(red) and B100(black) against (ΔP) across nozzle.$\rho_a = 22.7 kg/m^3$ (P_{amb} = 20 bar) round circles. $\rho_a = 34.6 kg/m^3$ (P_{amb} = 30 bar) solid Squares.

ble value of $\dot{M}$ for every condition. Ten(10) leading values had been utilized to determine the mean peak which is single reading from transitory region that represents the momentum flux for every condition.

- Any increment in the injection pressure effects in prolonged hydraulic delay period and premature injector closing.
- Increase in density inside chamber caused a decrement in determined $\dot{M}$ larger than that have been estimated because of change in back pressure which accompanies the change in ambient density(ρ_a). Spray did not emerge very far (0.5 mm) inside chamber before it was influenced by ambient density.
- B50 and B100 had a very identical almost the same momentum flux as simple diesel
- B50 and B100 have not shown any influence on the injection delay duration
- Fuel viscosities and densities have been calculated. Biodiesel has a greater density than simple diesel and greater viscosity
- The entire injected fuel mass in an injection period for all fuels was measured at three(3) different injection pressures. The higher densities of B50 and B100 have not shown any effect in total fuel injected mass, as total fuel injected mass for mixed fuels lesser than simple diesel fuel at every injection pressure
- The instantaneous $\dot{m}$ has been measured using the normalized technique. This normalized technique is based on momentum measurement and independently calculated the entire injected mass. The Instantaneous mass rate $\dot{m}$ shows a linear increment with ($\sqrt{\Delta P}$)
- Discharge coefficient(C_d) of nozzle has been calculated and observed alongside cavitation number(K). The B50 and B100 have a tendency to lesser discharge coefficient(C_d)value. There is not a single indication that nozzle is generating cavitation for any fuel at any condition tested. So, it is trusted that nozzle design competently suppressed the cavitation
- The injection velocities have been computed using average peak mass rate values and average peak momentum flux values. The B50 and B100 shown a higher injection velocity as compared to simple diesel spray. The velocity, viscosity and density have been utilized to calculate Reynolds number (Re_l) for every event. The Reynold numbers(Re_l) have shown some variations amongst all fuels at every condition. So, it is firmly established that here is an additional technique resulting in smaller discharge coefficient (C_d) and the higher injection velocities witnessed with B50 and B100
- It is witnessed that impact is relaxed with increment in injection pressure for every fuel tested, being revealing the effect of fuel sprays velocity, as lesser time is required by fuel spray to strike on sensor
- Momentum coefficients (C_m) have been calculated for fuel sprays and it is identical to coefficient of discharge. The B50 and B100 have minor to zero influence on momentum coefficient(C_m). So, it is apparent that an increment in ambient density lowers momentum coefficient (C_m) for every case.
- There in another parameter momentum efficiency which uses theoretical velocity and measurement of instantaneous mass of fuel spray. B50 and B100 have a greater momentum

efficiency(η_m) due to their higher injection velocity than simple diesel fuel.

- From above results it is determined that methods shown here gives a valid injection rate even with a theoretic policy and relying only on the momentum flux experimentations and total fuel mass injected. This concludes that only using these both measures a correct estimate may be achieved in event of having no existing services for direct injection rate measure
- At higher load conditions the CO emission for each fuel is lower. CO_2 and HC for both B50 and B100 increases with increment in biodiesel amount in their blends, however CO emissions drops down with rising biodiesel amount in blend
- As biodiesels contains greater oxygen content which leads to lesser CO emission with rising blends ratio because of complete combustion in diesel engine. Diesel engine operated by biodiesel will make good combustion because of existence of oxygen content in biodiesel molecule
- B50 shows a reduction in NOx emissions whereas B100 shows an increment in NOx emission
- B50 and B100 have significantly greater surface tension and viscosity as compared to simple diesel fuel which leads to variances in the atomization and spray structure. B50 and B100 are witnessed to exhibit greater spray cone angle and tip penetration as compared to simple diesel fuel. This study revealed that drops diameters are greater for B100 than for B50 as compared to simple diesel fuel. There are significant variations are witnessed between B50, B100 and diesel fuel. B100 spray exhibit a smaller lift off length, long liquid length and smaller ignition delay as compared to both B50 and Diesel fuel

CRediT authorship contribution statement

Muhammad Numan Atique: Conceptualization, Experimentation and writing-original draft preparation. **S. Imran:** Supervision. **Luqman Razzaq:** Methodology. **M.A. Mujtaba:** Formal analysis. **Saad Nawaz:** Software and validation. **M.A. Kalam:** Funding acquisition. **Manzoore Elahi M. Soudagar:** Reviewing and Editing. **Abrar Hussain:** Reviewing and Editing. **Ibham Veza:** Reviewing and Editing. **Attique Arshad:** Visualization.

Declaration of Competing Interest

The authors declare that they have no known competing financial interests or personal relationships that could have appeared to influence the work reported in this paper.

Acknowledgment

The authors would like to thank the Faculty of Engineering at the University of Malaya, Malaysia for their support through the research grant no GPF018A-2019.

References

[1] L. Razzaq et al, Modeling viscosity and density of ethanol-diesel-biodiesel ternary blends for sustainable environment, Sustain 12 (12) (2020), https://doi.org/10.3390/su12125186.

[2] C.Y. Lin, L.W. Chen, Comparison of fuel properties and emission characteristics of two- and three-phase emulsions prepared by ultrasonically vibrating and mechanically homogenizing emulsification methods, Fuel 87 (10–11) (2008) 2154–2161, https://doi.org/10.1016/j.fuel.2007.12.017.

[3] S.K. Grange, N.J. Farren, A.R. Vaughan, R.A. Rose, D.C. Carslaw, Strong temperature dependence for light-duty diesel vehicle NOx emissions, Environ. Sci. Technol. 53 (11) (2019) 6587–6596, https://doi.org/10.1021/acs.est.9b01024.

[4] M.K. Anser, Q. Abbas, I.S. Chaudhry, A. Khan, Optimal oil stockpiling, peak oil, and general equilibrium: case study of South Asia (oil importers) and Middle East (oil supplier), Environ. Sci. Pollut. Res. 27 (16) (2020) 19304–19313, https://doi.org/10.1007/s11356-020-08419-7.

[5] X. Duan, Z. Xu, X. Sun, B. Deng, J. Liu, Effects of injection timing and EGR on combustion and emissions characteristics of the diesel engine fuelled with acetone–butanol–ethanol/diesel blend fuels, Energy 231 (2021) 121069, https://doi.org/10.1016/j.energy.2021.121069.

[6] P. Boggavarapu, R.V. Ravikrishna, A review on atomization and sprays of biofuels for IC engine applications, Int. J. Spray Combust. Dyn. 5 (2) (2013) 85–121, https://doi.org/10.1260/1756-8277.5.2.85.

[7] L. Corral-Gómez, G. Rubio-Gómez, S. Martínez-Martínez, F. A. Sánchez-Cruz, Effect of diesel-biodiesel-ethanol blends on the spray macroscopic parameters in a common-rail diesel injection system, Fuel 241 (December 2018) (2019) 876–883, https://doi.org/10.1016/j.fuel.2018.12.081.

[8] S.K. Das, K. Kim, O. Lim, Experimental study on non-vaporizing spray characteristics of biodiesel-blended gasoline fuel in a constant volume chamber, Fuel Process. Technol. 178 (May) (2018) 322–335, https://doi.org/10.1016/j.fuproc.2018.05.009.

[9] F. Hussain et al, Enhancement in combustion, performance, and emission characteristics of a diesel engine fueled with Ce-ZnO nanoparticle additive added to soybean biodiesel blends, Energies 13 (17) (2020) 1–20, https://doi.org/10.3390/en13174578.

[10] M.E.M. Soudagar et al, Study of diesel engine characteristics by adding nanosized zinc oxide and diethyl ether additives in Mahua biodiesel–diesel fuel blend, Sci. Rep. 10 (1) (2020) 1–17, https://doi.org/10.1038/s41598-020-72150-z.

[11] G. Prabhakara Rao, V.R.K. Raju, S. Srinivasa Rao, Effect of fuel injection pressure and spray cone angle in di diesel engine using CONVERGETM CFD code, Procedia Eng. 127 (2015) 295–300, https://doi.org/10.1016/j.proeng.2015.11.372.

[12] K.M. Akkoli et al, Effect of injection parameters and producer gas derived from redgram stalk on the performance and emission characteristics of a diesel engine, Alexandria Eng. J. 60 (3) (2021) 3133–3142, https://doi.org/10.1016/j.aej.2021.01.047.

[13] H. Fayaz et al, Collective effect of ternary nano fuel blends on the diesel engine performance and emissions characteristics, Fuel 293 (October 2020) (2021) 120420, https://doi.org/10.1016/j.fuel.2021.120420.

[14] M.A. Mujtaba et al, Comparative study of nanoparticles and alcoholic fuel additives-biodiesel-diesel blend for performance and emission improvements, Fuel 279 (June) (2020) 118434, https://doi.org/10.1016/j.fuel.2020.118434.

[15] N. Nirmala, S.S. Dawn, C. Harindra, Analysis of performance and emission characteristics of Waste cooking oil and Chlorella variabilis MK039712.1 biodiesel blends in a single cylinder, four strokes diesel engine, Renew. Energy 147 (2020) 284–292, https://doi.org/10.1016/j.renene.2019.08.133.

[16] U. Rajak, P. Nashine, T.S. Singh, T.N. Verma, Numerical investigation of performance, combustion and emission characteristics of various biofuels, Energy Convers. Manag.

156 (August 2017) (2018) 235–252, https://doi.org/10.1016/j.enconman.2017.11.017.
[17] M.E.M. Soudagar et al, Effect of Sr@ZnO Nanoparticles and Ricinus Communis Biodiesel-diesel Fuel Blends on Modified CRDI Diesel Engine Characteristics vol. 215 (2021).
[18] E. Characteristics, SS symmetry Effect of Nano-Graphene Oxide and n-Butanol Fuel Additives Blended with Diesel — Nigella sativa Biodiesel Fuel Emulsion on Diesel, 2020.
[22] B.J. Bora, U.K. Saha, Emission reduction operating parameters for a dual-fuel diesel engine run on biogas and rice-bran biodiesel, J. Energy Eng. 143 (4) (2017) 04016064, https://doi.org/10.1061/(asce)ey.1943-7897.0000410.
[23] R.C.B. Correia et al., Productive Efficiency and Density and Viscosity Studies of Biodiesels from Vegetable Oil Mixtures, vol. 19, no. X, 2021.
[25] M.E. Ortner, W. Müller, I. Schneider, A. Bockreis, Environmental assessment of three different utilization paths of waste cooking oil from households, Resour. Conserv. Recycl. 106 (2016) 59–67, https://doi.org/10.1016/J.RESCONREC.2015.11.007.
[26] L. Razzaq et al, Engine performance and emission characteristics of palm biodiesel blends with graphene oxide nanoplatelets and dimethyl carbonate additives, J. Environ. Manage. 282 (December2020) (2021) 111917, https://doi.org/10.1016/j.jenvman.2020.111917.
[28] H.G. How, H.H. Masjuki, M.A. Kalam, Y.H. Teoh, In fl uence of injection timing and split injection strategies on performance, emissions, and combustion characteristics of diesel engine fueled with biodiesel blended fuels, Fuel 213 (August 2017) (2018) 106–114, https://doi.org/10.1016/j.fuel.2017.10.102.
[29] B. Mohan, W. Yang, S.K. Chou, Fuel injection strategies for performance improvement and emissions reduction in compression ignition engines – a review, Renew. Sustain. Energy Rev. 28 (2013) 664–676, https://doi.org/10.1016/j.rser.2013.08.051.
[30] Z. Yaakob, M. Mohammad, M. Alherbawi, Z. Alam, K. Sopian, Overview of the production of biodiesel from Waste cooking oil, Renew. Sustain. Energy Rev. 18 (2013) 184–193, https://doi.org/10.1016/j.rser.2012.10.016.
[31] C.D. Mandolesi De Araújo, C.C. De Andrade, E. De Souza, E. Silva, F.A. Dupas, Biodiesel production from used cooking oil: a review, Renew. Sustain. Energy Rev. 27 (2013) 445–452, https://doi.org/10.1016/j.rser.2013.06.014.
[32] D. Suhendra, E.R. Gunawan, A.D. Nurita, D. Komalasari, T. Ardianto, Optimization of the enzymatic synthesis of biodiesel from Terminalia cattapa L. Kernel oil using response surface methodology, J. Oleo Sci. 66 (3) (2017) 209–215, https://doi.org/10.5650/jos.ess16167.
[33] M.A. Mujtaba et al, Ultrasound-assisted process optimization and tribological characteristics of biodiesel from palm-sesame oil via response surface methodology and extreme learning machine – Cuckoo search, Renew. Energy 158 (2020) 202–214, https://doi.org/10.1016/j.renene.2020.05.158.
[34] Sahar et al, Biodiesel production from waste cooking oil: an efficient technique to convert waste into biodiesel, Sustain. Cities Soc. 41 (2018) 220–226, https://doi.org/10.1016/J.SCS.2018.05.037.
[35] W. Jindapon, S. Ruengyoo, P. Kuchonthara, C. Ngamcharussrivichai, T. Vitidsant, Continuous production of fatty acid methyl esters and high-purity glycerol over a dolomite-derived extrudate catalyst in a countercurrent-flow trickle-bed reactor, Renew. Energy 157 (2020) 626–636, https://doi.org/10.1016/j.renene.2020.05.066.
[36] Y. Zheng, M.S. Shadloo, H. Nasiri, A. Maleki, A. Karimipour, I. Tlili, Prediction of viscosity of biodiesel blends using various artificial model and comparison with empirical correlations, Renew. Energy 153 (2020) 1296–1306, https://doi.org/10.1016/j.renene.2020.02.087.
[39] M.V. van der Seijs, E.A. Pasma, D.D. van den Bosch, M.W.F. Wernsen, A benchmark structure for validation of experimental substructuring, transfer path analysis and source characterisation techniques, Conf. Proc. Soc. Exp. Mech. Ser. 4 (2017) 295–305, https://doi.org/10.1007/978-3-319-54930-9_26.
[40] C. Zhai, Y. Jin, K. Nishida, Y. Ogata, Diesel spray and combustion of multi-hole injectors with micro-hole under ultra-high injection pressure – Non-evaporating spray characteristics, Fuel 283 (September) (2020) 2021, https://doi.org/10.1016/j.fuel.2020.119322.
[41] A. Cavicchi, L. Postrioti, F. Berni, S. Fontanesi, R. Di Gioia, Evaluation of hole-specific injection rate based on momentum flux measurement in GDI systems, Fuel 263 (June) (2020), https://doi.org/10.1016/j.fuel.2019.116657.
[42] M.D. Sirignano, V. Nair, B.L. Emerson, J. Seitzman, T.C. Lieuwen, Nitrogen oxide emissions from premixed reacting jets in a vitiated crossflow, Combust. Sci. Technol. 192 (7) (2020) 1389–1419, https://doi.org/10.1080/00102202.2020.1748016.
[43] Z. Chen et al, Experimental study on the effect of nozzle geometry on string cavitation in real-size optical diesel nozzles and spray characteristics, Fuel 232 (May) (2018) 562–571, https://doi.org/10.1016/j.fuel.2018.05.132.
[44] D.R. Emberson, Diesel fuel and Diesel fuel with Water Emulsions Spray and Combustion Characterization, 2015.
[45] L.Y. Zhou, S.F. Dong, H.F. Cui, X.W. Wu, F.Y. Xue, F.Q. Luo, Measurements and analyses on the transient discharge coefficient of each nozzle hole of multi-hole diesel injector, Sensors Actuators, A Phys. 244 (2016) 198–205, https://doi.org/10.1016/j.sna.2016.04.017.
[46] R. Payri, S. Ruiz, F.J. Salvador, J. Gimeno, On the dependence of spray momentum flux in spray penetration: momentum flux packets penetration model, J. Mech. Sci. Technol. 21 (7) (2007) 1100–1111, https://doi.org/10.1007/BF03027660.
[47] C. Cen, H. Wu, C. fon Lee, F. Liu, Y. Li, Experimental investigation on the characteristic of jet break-up for butanol droplet impacting onto a heated surface in the film boiling regime, Int. J. Heat Mass Transf. 123 (2018) 129–136, https://doi.org/10.1016/j.ijheatmasstransfer.2018.02.059.
[48] F.J. Salvador, J.J. Lopez, J. De la Morena, M. Crialesi-Esposito, Experimental investigation of the effect of orifices inclination angle in multihole diesel injector nozzles. Part 1 – Hydraulic performance, Fuel 213 (2018) 207–214, https://doi.org/10.1016/j.fuel.2017.04.019.
[49] M. Wei et al, Experimental study of cavitation formation and primary breakup for a biodiesel surrogate fuel (methyl butanoate) using transparent nozzle, Fuel 203 (2017) 690–699, https://doi.org/10.1016/j.fuel.2017.05.022.
[50] Y. Gao, M. Wei, F. Yan, L. Chen, G. Li, L. Feng, Effects of cavitation flow and stagnant bubbles on the initial temporal evolution of diesel spray, Exp. Therm. Fluid Sci. 87 (2017) 69–79, https://doi.org/10.1016/j.expthermflusci.2017.04.029.
[51] F.J. Salvador, M. Carreres, D. Jaramillo, J. Martínez-López, Analysis of the combined effect of hydrogrinding process and inclination angle on hydraulic performance of diesel injection nozzles, Energy Convers. Manag. 105 (2015) 1352–1365, https://doi.org/10.1016/j.enconman.2015.08.035.
[52] M. Medina, A. Bautista, M. Wooldridge, R. Payri, The effects of injector geometry and operating conditions on spray mass, momentum and development using high-pressure gasoline, Fuel 294 (February) (2021) 120468, https://doi.org/10.1016/j.fuel.2021.120468.
[53] R. Zhang, B. Zhang, Q. Lv, J. Li, P. Guo, Effects of droplet shape on impact force of low-speed droplets colliding with solid surface, Exp. Fluids 60 (4) (2019), https://doi.org/10.1007/s00348-019-2712-7.
[54] D.R. Emberson, B. Ihracska, S. Imran, A. Diez, M. Lancaster, T. Korakianitis, Hydraulic characterization of Diesel and water

emulsions using momentum flux, Fuel 162 (2015) 23–33, https://doi.org/10.1016/j.fuel.2015.08.016.

[56] R. Payri, F.J. Salvador, J. De la Morena, V. Pagano, Experimental investigation of the effect of orifices inclination angle in multihole diesel injector nozzles. Part 2 – Spray characteristics, Fuel 213 (July) (2018) 215–221, https://doi.org/10.1016/j.fuel.2017.07.076.

[57] B. Mohan, J. Du, J. Sim, W.L. Roberts, Hydraulic characterization of high-pressure gasoline multi-hole injector, Flow Meas. Instrum. 64 (2018) 133–141, https://doi.org/10.1016/j.flowmeasinst.2018.10.017.

[58] R. Payri, A. García, V. Domenech, R. Durrett, A.H. Plazas, An experimental study of gasoline effects on injection rate, momentum flux and spray characteristics using a common rail diesel injection system, Fuel 97 (2012) 390–399, https://doi.org/10.1016/j.fuel.2011.11.065.

[60] F.J. Salvador, J. De la Morena, J. Martínez-López, D. Jaramillo, Assessment of compressibility effects on internal nozzle flow in diesel injectors at very high injection pressures, Energy Convers. Manag. 132 (2017) 221–230, https://doi.org/10.1016/j.enconman.2016.11.032.

[63] L. Li, H. Yan, H. Zhang, J. Li, Numerical simulation and experimental research of the flow force and forced vibration in the nozzle-flapper valve, Mech. Syst. Signal Process. 99 (2018) 550–566, https://doi.org/10.1016/j.ymssp.2017.06.024.

[64] A. Ferrari, A. Mittica, F. Paolicelli, P. Pizzo, Hydraulic characterization of solenoid-actuated injectors for diesel engine common rail systems, Energy Procedia 101 (September) (2016) 878–885, https://doi.org/10.1016/j.egypro.2016.11.111.

[67] M. Ghiji, L. Goldsworthy, P.A. Brandner, V. Garaniya, P. Hield, Analysis of diesel spray dynamics using a compressible Eulerian/VOF/LES model and microscopic shadowgraphy, Fuel 188 (2017) 352–366, https://doi.org/10.1016/j.fuel.2016.10.041.

[68] T.Y. Kim, S.H. Lee, Combustion and emission characteristics of wood pyrolysis oil-butanol blended fuels in a di diesel engine, Int. J. Automot. Technol. 13 (2) (2012) 293–300, https://doi.org/10.1007/s12239.

[71] R. Payri, G. Bracho, J.A. Soriano, P. Fernández-Yáñez, O. Armas, Nozzle rate of injection estimation from hole to hole momentum flux data with different fossil and renewable fuels, Fuel 279 (May) (2020) 118404, https://doi.org/10.1016/j.fuel.2020.118404.